Molecular Therapy
Oncolytics
Original Article

OCT4B1 Promoted EMT and Regulated the Self-Renewal of CSCs in CRC: Effects Associated with the Balance of miR-8064/PLK1

Jun-min Zhou,[1,3] Shui-qing Hu,[1,3] Hang Jiang,[1] Yi-lin Chen,[1] Ji-hong Feng,[2] Zheng-quan Chen,[1] and Kun-ming Wen[1]

[1]Department of Gastrointestinal Surgery, The Affiliated Hospital of Zunyi Medical University, Zunyi, Guizhou 563000, China; [2]Department of Oncology, The Affiliated Hospital of Zunyi Medical University, Zunyi, Guizhou 563000, China

Cancer stem cells (CSCs) are the main cause of tumor generation, recurrence, metastasis, and therapy failure in various malignancies including colorectal cancer (CRC). Accumulating evidence suggests that tumor cells can acquire CSC characteristics through the epithelial-mesenchymal transition (EMT) process. However, the molecular mechanism of CSCs remains unclear. OCT4B1 is a transcript of OCT4, which is initially expressed in embryonic stem and carcinoma cells, and is involved in the regulation and maintenance of an undifferentiated state of stem cells. In this study, three-dimensional (3D) microspheres were confirmed as CRC stem cells. Compared with that of parental cells, their self-renewal ability was significantly increased, and OCT4B1 expression was increased and promoted the EMT process. The knockdown of OCT4B1 decreased the self-renewal of CSCs and reversed EMT. Moreover, OCT4B1 induced the expression of Polo-like kinase 1 (PLK1), which is a key regulator of EMT in tumor cells. Further examination showed that OCT4B1 regulated the miR-8064/PLK1 balance to exert its function. Taken together, our data suggest that OCT4B1 may be involved in regulating the self-renewal of colorectal CSCs through EMT, which is at least partially due to the miR-8064/PLK1 balance. This study indicates that OCT4B1 is a potential therapeutic target for CRC by targeting CSCs.

INTRODUCTION

Colorectal cancer (CRC) is the third most common cancer and the fourth leading cause of cancer death in the world.[1] Recently, it has been reported that CRC has exhibited an increasing trend in patients <50 years old.[2] Surgery and radiochemotherapy are the main treatment methods for CRC patients. Although surgical and radiochemotherapy techniques have been continuously improved in recent years, the 5-year survival rate of CRC patients remains unsatisfactory. According to reports, the 5-year survival rate of metastatic CRC patients is approximately 12.5%, and the cause is significantly correlated with the recurrence and metastasis of cancer.[3] A large number of studies have shown that the existence of cancer stem cells (CSCs) is the main cause of tumor recurrence and metastasis.[4,5] CSCs are characterized by differentiation potential, self-renewal, tumorigenicity, and enrichment of CSC markers. Furthermore, CSCs have high telomerase activity and are insensitive to radiotherapy, chemotherapy, and epithelial-mesenchymal transition (EMT) labeling.[6,7] Studies have found that tumor cells can acquire stem cell characteristics in the EMT process. After EMT, tumor invasion, migration, and anti-apoptotic ability are enhanced, and the degree of malignancy is increased.[8] Therefore, there is a need to study the specific mechanism of the EMT process in regulating CSCs to seek new therapeutic targets for CRC and improve the prognosis and quality of life of patients.

EMT, which was first proposed by Greenberg and Hay in 1982, refers to the process of transforming epithelial cells into mesenchymal-like cells during embryonic development or pathological conditions and is accompanied by various phenomena, including the disappearance of cell polarity, decreased contact between cells, increased cell invasion and migration, and decreased cell adhesion.[9] EMT is triggered by the activation of the extracellular matrix and various growth factors, such as transforming growth factor-β (TGF-β), epidermal growth factor (EGF), b-fibroblast growth factor (b-FGF), and various transcription factors, such as Snail, Slug, and Twist. In this process, cells lose their epithelial phenotype and obtain a mesenchymal phenotype, which is involved in organ and tissue formation, wound repair, organ fibrosis, and cancer formation.[9] Charpentier et al.[10] found that breast CSCs had EMT characteristics, with significantly enhanced migration and invasion. In the process of malignant tumor recurrence, metastasis, and drug resistance, EMT occurred with loss of the epithelial phenotype and the attainment of the mesenchymal phenotype, whereas tumor cells obtained a CSC phenotype in the EMT process.[11–13] EMT is a mechanism that gives rise to the invasive and metastatic phenotypes of CSCs.[14,15]

Received 26 October 2018; accepted 20 August 2019;
https://doi.org/10.1016/j.omto.2019.08.004.

[3]These authors contributed equally to this work.

Correspondence: Kun-ming Wen, Department of Gastrointestinal Surgery, The Affiliated Hospital of Zunyi Medical University, 149 DaLian Road, Zunyi, Guizhou 563000, China.
E-mail: 381224619@qq.com

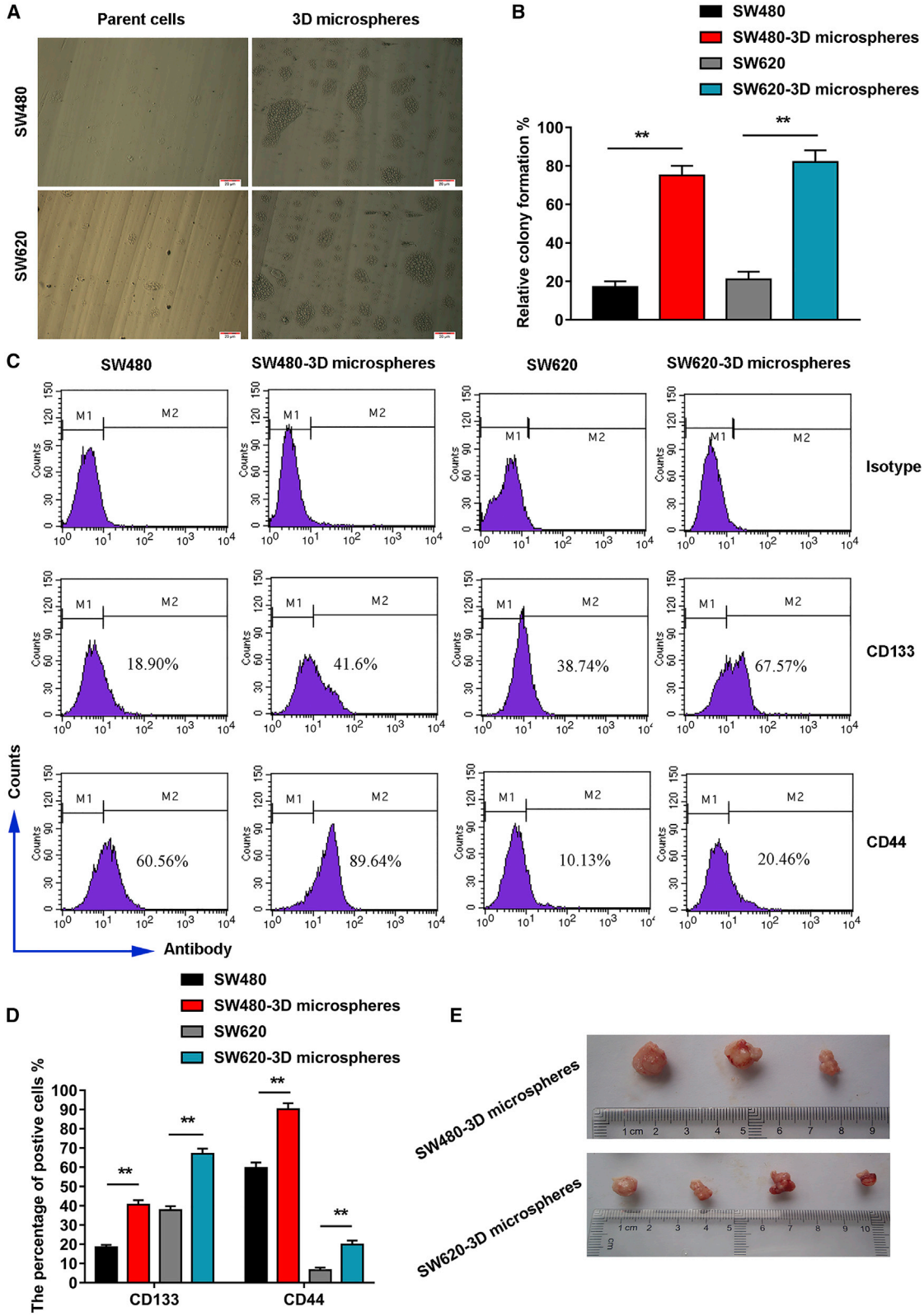

(legend on next page)

OCT4, also known as POU5F1, is a protein that encodes the *POU5F1* gene in humans. OCT4 is a homeobox transcription factor of the POU family and a key regulator of the self-renewal of undifferentiated embryonic stem cells (ESCs). OCT4 is highly expressed in many cancers, including CRC cells, and it participates in the regulation of CSCs and tumor EMT processes.[16–19] Human OCT4 contains five exons on chromosome 6 and is capable of producing at least three variants (A, B, and B1) by selective cleavage.[20] OCT4B1 is initially expressed in ESCs and embryonic carcinoma cells, and is involved in the regulation and maintenance of an undifferentiated state of stem cells.[21] Subsequent studies have revealed that its expression is elevated and plays a pro-oncogenic role in various cancers, including CRC, gastric cancer, and bladder cancer.[20,22–24] OCT4B1 contributes to tumorigenesis in cancer cells by inhibiting a large number of pro-apoptotic genes and increasing the expression of anti-apoptotic genes.[25] Malek H. Asadi et al.[22] found that OCT4B1 was highly expressed in gastric cancer and played an anti-apoptotic role, and it might be used as a tumor marker for gastric cancer or other tumors. Maria Gazouli et al.[20] found that high expression levels of OCT4B1 contribute to the progression of colon cancer by analyzing OCT4B1 expression in colon cancer samples through histological grading and differentiation. Furthermore, the elevated expression of OCT4B1 helps maintain the undifferentiated state of cancer cells and increases their ability to self-renew and proliferate, suggesting that OCT4B1 overexpression can lead to poor prognosis in CRC patients. In our previous studies on OCT4B1 overexpression in CRC SW480 and SW620 cells, it was revealed that the migration and invasion of CRC cells increased, the resistance to the chemotherapeutic drug oxaliplatin increased, the expression of the epithelial marker E-cadherin was significantly downregulated, and the expression of the mesenchymal markers N-cadherin and vimentin was significantly upregulated, suggesting that OCT4B1 could induce EMT in parental CRC cells.[26] Spyros I. Papamichos et al.[24] mentioned in a report on OCT4 and its subtypes in stem cells that OCT4B1 is involved in the regulation of self-renewal in ESCs. Thus far, there has been no report on whether OCT4B1 can regulate CSCs.

The aim of the present study was to determine whether OCT4B1 can enable colorectal CSCs to acquire self-renewal capacity through EMT. Furthermore, the present study also investigated the indicator Polo-like kinase 1 (PLK1), which regulates cancer EMT downstream of OCT4B1, and screened and verified miRNAs that regulate the expression of PLK1 using miRNA microarray technology to elucidate the regulatory mechanism of OCT4B1.

RESULTS

3D Microspheres Exhibit CSC Properties

The SW480-3D and SW620-3D microspheres, which were obtained from a suspension culture of the human CRC cell lines SW480 and SW620, respectively, grew in suspension, which was densely arranged and had a significantly increased volume. To verify the self-renewal of the 3D microspheres, we performed a colony formation assay. SW480-3D microsphere cells, SW620-3D microsphere cells, their parental SW480 cells, and SW620 cells were all cultured in soft agar medium. SW480-3D microsphere cells and their parent SW480 cells had colony formation rates of 75% ± 5% and 17% ± 3%, respectively, whereas SW620-3D microspheres and their parental SW620 cells had colony formation rates of 82% ± 6% and 21% ± 4%, respectively. The colony-forming rate of SW480-3D and SW620-3D microsphere cells was significantly higher than that of their parental cells (Figures 1A and 1B).

Next, 3D microspheres and their parental cells were compared for the expression of the cell surface CRC stem cell markers CD133 and CD44. Flow cytometric analysis revealed that CD133 was expressed in 40.58% ± 2.32% of SW480-3D microspheres, 67.08% ± 2.59% of SW620-3D microspheres, 18.45% ± 1.21% of SW480 cells, and 37.74% ± 2.01% of SW620 cells. In addition, the flow cytometric analysis revealed that CD44 was expressed in 90.21% ± 3.11% of SW480-3D microspheres, 19.80% ± 2.12% of SW620-3D microspheres, 59.61% ± 2.87% of SW480 cells, and 9.58% ± 1.34% of SW620 cells. This result shows that the expression levels of CD133 and CD44 were significantly elevated in 3D microspheres when compared with their parental cells (Figures 1C and 1D).

Furthermore, the tumorigenic capacity of 3D microspheres and their parental cells was tested by subcutaneous inoculation of approximately 10^3 cells from each cell line into the left armpit of non-obese diabetic/severe combined immunodeficient (NOD/SCID) mice (five mice/group). After 6 weeks, the mice in the SW480-3D microsphere group formed three tumors out of five mice, and mice in the SW620-3D microsphere group formed four tumors out of five mice

Figure 1. Self-Renewal Ability of 3D Microspheres

(A) The results of soft agar clones of SW480 parent cells, SW480-3D microspheres, SW620 parent cells, and SW620-3D microspheres. Scale bars: 20 μm. (B) The histogram shows that the colony formation rates of SW480-3D and SW620-3D microspheres were significantly higher than those of their parent cells. Each bar represents the mean values ± SD of three independent experiments. **$p < 0.01$. (C) 3D microspheres were enriched for $CD133^+$ and $CD44^+$ cells. Flow cytometric analysis showed that both 3D microspheres were enriched for cells that expressed CD133 and CD44 when compared with the parental cell lines. A total of 41.63% of the SW480-3D microspheres and 67.57% of the SW620-3D microspheres expressed CD133 relative to 18.90% of the SW480 cells and 38.74% of the SW620 cells, whereas 89.64% of the SW480-3D microspheres and 20.46% of the SW620-3D microspheres expressed CD44 relative to 60.56% of the SW480 cells and 10.13% of the SW620 cells. Cytometric analysis plots using isotype control antibodies are provided as staining controls. (D) The histogram shows the percentage of CD44- and CD133-positive SW480 cells, SW480-3D microspheres, SW620 cells, and SW620-3D microspheres detected by flow cytometry. Each bar represents the mean values ± SD of three independent experiments. **$p < 0.01$. (E) The tumorigenic capacity of 3D microspheres in NOD/SCID mice: three tumors were harvested from five NOD/SCID mice receiving injections of SW480-3D microspheres, and four tumors were harvested from five NOD/SCID mice receiving injections of SW620-3D microspheres, but mice in the SW480 and SW620 groups did not manifest any detectable tumors under the same conditions at the end of the experiment.

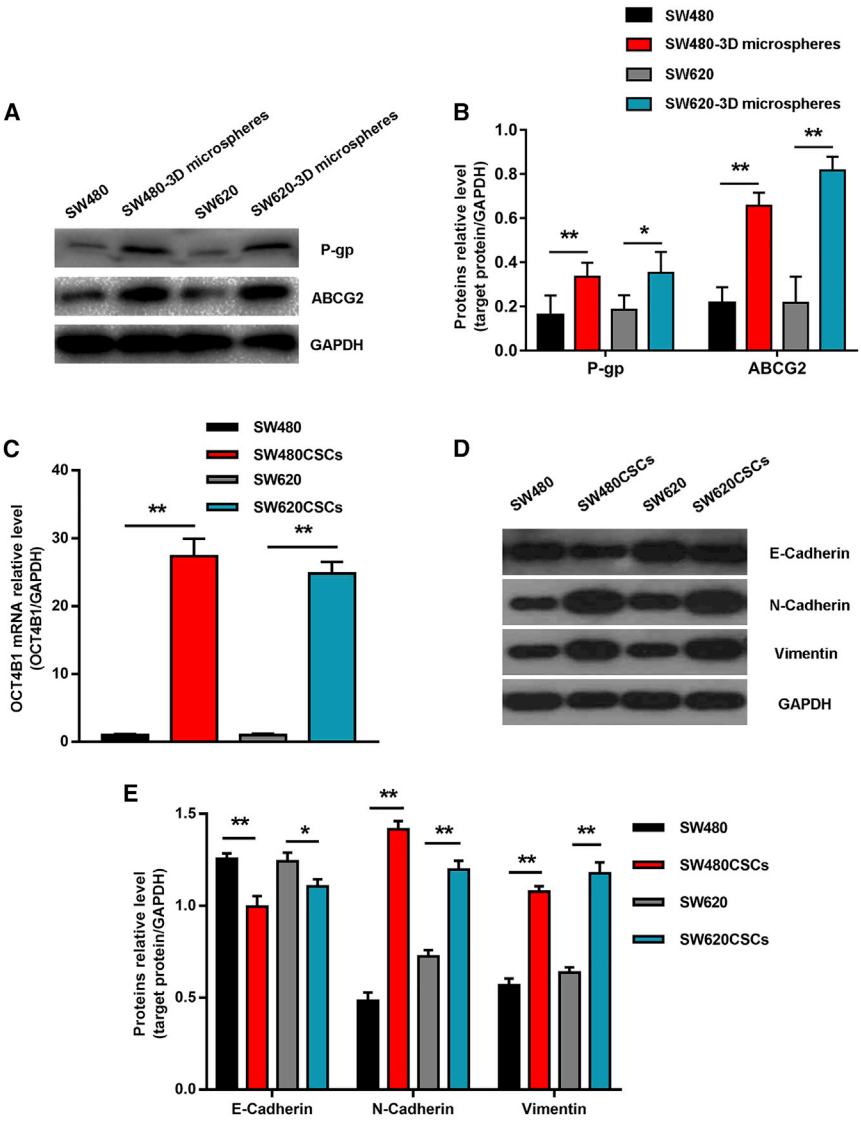

Figure 2. The Expression Levels of P-gp, ABCG2, and OCT4B1 Increased in Colorectal CSCs, Which Could Have Underwent the EMT Process

(A and B) The protein expression levels of P-gp and ABCG2 in SW480-3D microspheres (SW480CSCs), SW620-3D microspheres (SW620CSCs), and their parental cancer cells were analyzed by western blot (A) and calculated (B). (C) The mRNA expression levels of OCT4B1 in SW480CSCs, SW620CSCs, and their parental cancer cells were analyzed by qRT-PCR. (D and E) The protein expression levels of E-cadherin, N-cadherin, and vimentin in SW480CSCs, SW620CSCs, and their parental cancer cells were analyzed by western blot (D) and calculated (E). Each bar represents the mean values ± SD of three independent experiments. *$p < 0.05$, **$p < 0.01$.

(Figure 1E). However, mice in the SW480 and SW620 groups did not manifest any detectable tumors under these conditions, suggesting that the 3D microspheres were more tumorigenic than their parental cells.

In addition, western blotting was used to examine the expression of the chemoresistant proteins P-gp and ABCG2, which play important roles in the drug resistance of CRC.[27,28] When compared with that in the parental cancer cells, the protein expression of P-gp and ABCG2 in SW480-3D and SW620-3D microsphere cells increased significantly (Figures 2A and 2B). The results suggested that 3D microspheres have acquired drug resistance.

SW480-3D and SW620-3D microspheres have the characteristics of CSCs. Compared with their parental cells, it was found that SW480-3D and SW620-3D microspheres had increased colony formation ability, enriched colorectal CSC markers, enhanced tumorigenic capacity in NOD/SCID mice, and acquired drug resistance. Therefore, we termed the SW480-3D and SW620-3D microspheres with tumor stem cell characteristics as SW480CSCs and SW620CSCs, respectively.

Upregulation of OCT4B1 Expression in Colorectal CSCs Accompanies the EMT Process

In addition to the assessment of colorectal CSC self-renewal, the expression of OCT4B1, an essential regulator of the self-renewal of undifferentiated ESCs, was investigated. The relative mRNA expression of OCT4B1 in the SW480, SW480CSCs, SW620, and SW620CSCs groups was 1.00 ± 0.15, 27.36 ± 2.56, 1.00 ± 0.21, and 24.82 ± 1.67, respectively, as detected by qRT-PCR. The OCT4B1 mRNA expression levels were 27- and 25-fold higher in SW480CSCs and SW620CSCs, respectively, when compared with their parental cancer cells (Figure 2C). EMT markers in SW480, SW480CSCs, SW620, and SW620CSCs were detected by western blot. When compared with that in the parental cancer cells, the protein expression of the epithelial cell marker E-cadherin in SW480CSCs and SW620CSCs decreased significantly, whereas the protein expression of the mesenchymal cell markers N-cadherin and vimentin increased significantly (Figures 2D and 2E). This suggests that the transformation of SW480 and SW620 to SW480CSCs and SW620CSCs, respectively, underwent the EMT process.

Reduced Self-Renewal in Colorectal CSCs after Silencing the OCT4B1 Gene

The OCT4B1 gene was silenced in SW480CSCs and SW620CSCs by OCT4B1-short hairpin RNA (shRNA)-lentivirus vector (LV)

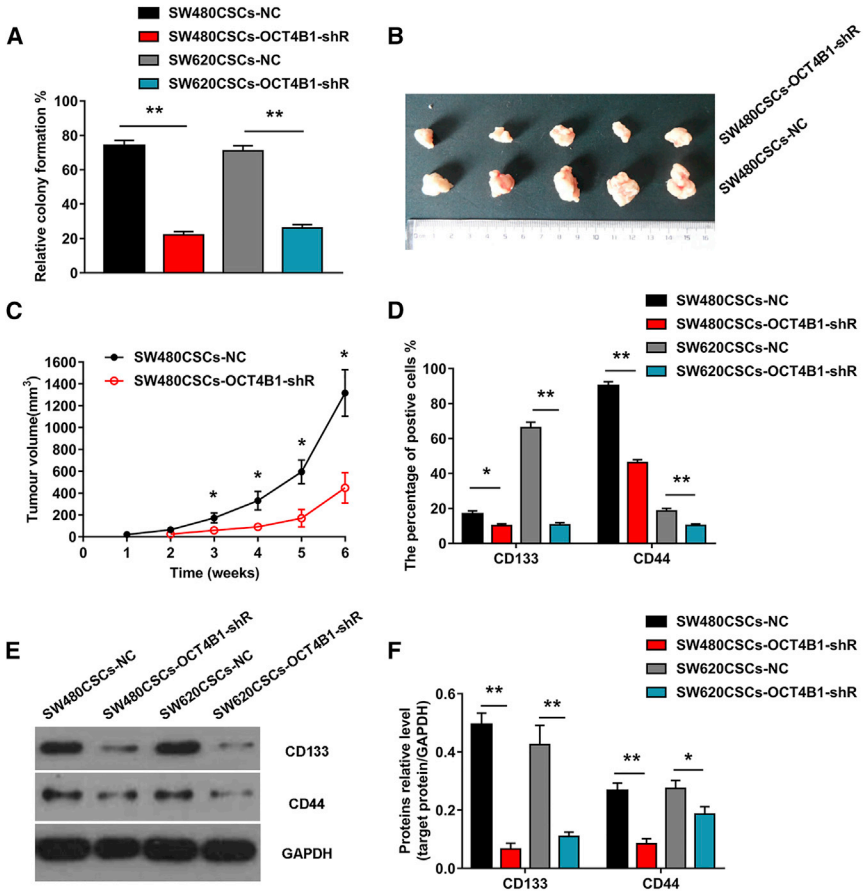

Figure 3. The Self-Renewal of Colorectal CSCs Decreased after Silencing the *OCT4B1* Gene

(A) The relative colony formation rates of the SW480CSCs-NC group, SW480CSCs-OCT4B1-shR group, SW620CSCs-NC group, and SW620CSCs-OCT4B1-shR group. (B and C) The tumor growth of nude mice in the SW480CSCs-NC and SW480CSCs-OCT4B1-shR groups is shown. SW480CSCs were treated with NC-GFP-LV or OCT4B1-shRNA-LV, and then approximately 1×10^6 cells were inoculated subcutaneously into the flanks of NOD/SCID mice 48 h postinfection. Tumors were measured weekly and harvested at 6 weeks post inoculation (B). The cells treated with OCT4B1-shRNA-LV formed significantly smaller tumors than the cells treated with NC-GFP-LV under similar experimental conditions (C) (n = 5/group; *p < 0.05 between SW480CSCs-NC group and SW480CSCs-OCT4B1-shR group). (D) The proportions of CD44- and CD133-positive cells in the RNAi group and NC group were analyzed by flow cytometry. (E and F) The protein expression of the colorectal CSC markers CD44 and CD133 in the OCT4B1-shR group and NC group, respectively, was detected by western blot (E) and calculated (F). Each bar represents the mean values ± SD of three independent experiments. *p < 0.05, **p < 0.01.

transfection. First, the knockdown efficiency was tested. The experimental group (group OCT4B1-shR) was transfected with OCT4B1-shRNA-LV, and the negative control (NC) group was transfected with NC-GFP-LV. These two groups showed green fluorescence under a fluorescence microscope after 3 days of transfection, suggesting that cells in the OCT4B1-shR group and NC group were successfully transfected (Figure S1A). The relative mRNA expression of OCT4B1 in the SW480CSCs-NC, SW480CSCs-OCT4B1-shR, SW620CSCs-NC, and SW620CSCs-OCT4B1-shR groups was 1.00 ± 0.12, 0.23 ± 0.03, 1.00 ± 0.06, and 0.18 ± 0.04, respectively, as detected by qRT-PCR. Compared with that in the NC group transfected with NC-LV, the mRNA level of OCT4B1 in the shRNA group significantly decreased after transfection with OCT4B1-sh-RNA-LV (Figure S1B). Furthermore, the same trend was observed for OCT4B1 protein levels detected by western blot analysis (Figures S1C and S1D). These results suggest that the OCT4B1 gene in SW480CSCs and SW620CSCs was silenced successfully.

The colony formation rates of the SW480CSCs-OCT4B1-shR group and SW480CSCs-NC group were 22% ± 2% and 74% ± 3%, respectively. In addition, the colony formation rates of the SW620CSCs-OCT4B1-shR group and SW620CSCs-NC group were 26% ± 2% and 71% ± 3%, respectively. For the colony formation rate of the SW480CSCs-OCT4B1-shR group, the rate of the SW620CSCs-OCT4B1-shR group was significantly lower than those of the corresponding NC groups (Figure 3A). The colony-forming ability of SW480CSCs and SW620CSCs after silencing the *OCT4B1* gene significantly decreased. NOD/SCID mice injected with shRNA-treated CSCs (SW480CSCs-OCT4B1-shR and SW620CSCs-OCT4B1-shR) formed no tumors out of five mice, whereas mice injected with SW480CSCs-NC formed four tumors out of five mice, and SW620CSCs-NC cells formed five tumors out of five mice. Furthermore, the tumorigenic capacity of shRNA-treated and NC-treated CSCs was tested through the subcutaneous inoculation of approximately 10^6 cells from each cell line into the left flank of nude mice (five mice per group). After 6 weeks, each group formed tumors out of five mice, but the tumor volumes of the SW480CSCs-OCT4B1-shR group were significantly smaller than those obtained from the corresponding NC-treated CSCs mice (Figures 3B and 3C). Based on this finding, it can be concluded that shRNA-treated CSCs had a weakened tumorigenic capacity and tumor growth inhibitory effects in NOD/SCID mice and nude mice.

The proportion of $CD133^+$ cells in the SW480CSCs-OCT4B1-shR group was reduced from 16.71% ± 1.89% in the SW480CSCs-NC group to 10.21% ± 1.01%, as determined by flow cytometry, and the proportion of $CD44^+$ cells in the SW480CSCs-OCT4B1-shR

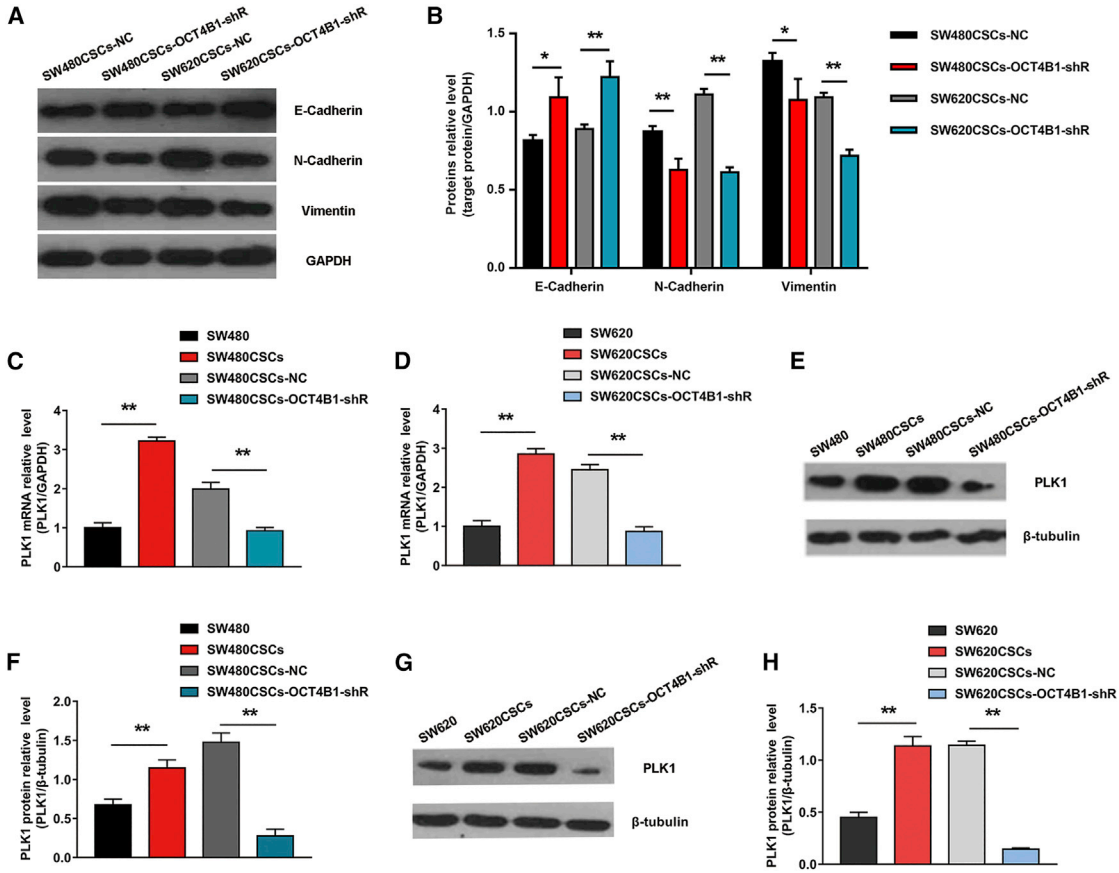

Figure 4. The Reversal of EMT in Colorectal CSCs after Silencing the *OCT4B1* Gene

(A and B) The protein expression levels of E-cadherin, N-cadherin, and vimentin in SW480CSCs-NC, SW480CSCs-OCT4B1-shR, SW620CSCs-NC, and SW620CSCs-OCT4B1-shR groups were detected by western blot (A) and calculated (B). (C) The mRNA levels of PLK1 in the SW480, SW480CSCs, SW480CSCs-NC, and SW480CSCs-OCT4B1-shR groups were detected by qRT-PCR. (D) The mRNA levels of PLK1 in the SW620, SW620CSCs, SW620CSCs-NC, and SW620CSCs-OCT4B1-shR groups were detected by qRT-PCR. (E and F) The protein expression of PLK1 in the SW480, SW480CSCs, SW480CSCs-NC, and SW480CSCs-OCT4B1-shR groups was detected by western blot (E) and calculated (F). (G and H) The protein expression of PLK1 in the SW620, SW620CSCs, SW620CSCs-NC, and SW620CSCs-OCT4B1-shR groups was detected by western blot (G) and calculated (H). Each bar represents the mean values ± SD of three independent experiments. *$p < 0.05$, **$p < 0.01$.

group was reduced from 90.05% ± 2.41% in the control group to 46.32% ± 1.54%. The proportion of $CD133^+$ cells in the SW620CSCs-OCT4B1-shR group was reduced from 66.12% ± 3.21% in the SW620CSCs-NC group to 10.56% ± 1.23%, as determined by flow cytometry, and the proportion of $CD44^+$ cells in the SW620CSCs-OCT4B1-shR group was reduced from 18.56% ± 1.47% in the control group to 10.31% ± 0.81% (Figure 3D). Consistent with the flow cytometry results, western blot detection revealed that the protein expression of CD133 and CD44 in the SW480CSCs-OCT4B1-shR and SW620CSCs-OCT4B1-shR groups decreased significantly when compared with that in the SW480CSCs-NC and SW620CSCs-NC groups (Figures 3E and 3F). After shRNA interference targeting OCT4B1, the colony-forming ability of the cells was significantly weakened, the tumorigenic capacity *in vivo* was significantly reduced, and the colorectal CSC markers decreased. Based on these findings, it could be concluded that inhibition of OCT4B1 reduced the self-renewal of SW480CSCs and SW620CSCs.

The Reversal of EMT in Colorectal CSCs after Silencing the *OCT4B1* Gene

Compared with that in SW480CSCs-NC and SW620CSCs-NC cells, the protein expression of the epithelial cell marker E-cadherin in SW480CSCs-OCT4B1-shR and SW620CSCs-OCT4B1-shR cells significantly increased, whereas the protein expression of the interstitial cell markers N-cadherin and vimentin was significantly decreased (Figures 4A and 4B), suggesting that the silencing of OCT4B1 participated in the reversal of EMT in SW480CSCs-OCT4B1-shR and SW620CSCs-OCT4B1-shR cells. Overall, the self-renewal of SW480CSCs and SW620CSCs was reduced after silencing the *OCT4B1* gene. These results indicate that inhibition of OCT4B1 reduced the self-renewal of CSCs through the reversal of the EMT process.

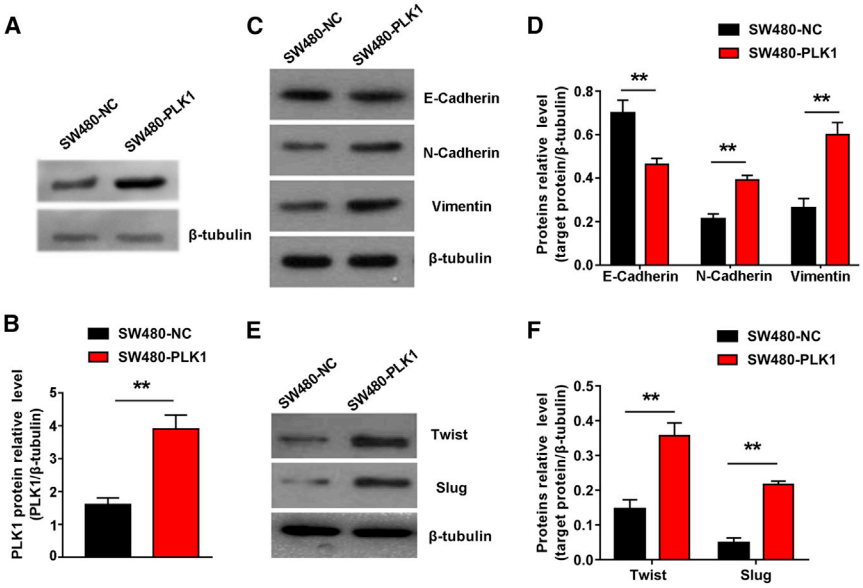

Figure 5. Overexpression of PLK1 in SW480 Cells Induces EMT

(A and B) The protein expression of PLK1 in SW480 cells transduced with a PLK1-overexpressing virus or NC virus was detected by western blot (A) and calculated (B). (C and D) The protein expression of N-cadherin, E-cadherin, and vimentin in the SW480-PLK1 group and NC group was detected by western blot (C) and calculated (D). (E and F) The protein expression levels of Twist and Slug in the SW480-PLK1 group and NC group were detected by western blot (E) and calculated (F). Each bar represents the mean values ± SD of three independent experiments. **$p < 0.01$.

Correlation between OCT4B1 mRNA Expression and the Clinicopathological Characteristics of CRC Patients

To investigate the clinicopathological significance of OCT4B1, we detected OCT4B1 mRNA in 53 CRC tissue specimens by qRT-PCR. Patients were divided into two groups according to the median expression level of OCT4B1 mRNA. As shown in Table S2, we found that upregulated OCT4B1 mRNA expression was significantly associated with tumor node metastasis (TNM) stage ($p = 0.001$), tumor infiltration ($p = 0.013$), lymph node metastasis ($p = 0.014$), and distant metastasis ($p = 0.021$). Other clinical characteristics such as gender ($p = 0.875$), age ($p = 0.893$), tumor site ($p = 0.04$), tumor size ($p = 0.697$), tumor differentiation ($p = 0.071$), and the preoperative carcinoembryonic antigen (CEA) level ($p = 0.336$) were not associated with the expression of OCT4B1 mRNA.

OCT4B1 Regulates PLK1 Expression

The mRNA expression of PLK1 in the SW480CSCs and SW620CSCs groups was higher than that in their parental cancer cells, and the mRNA expression of PLK1 in the SW480CSCs-OCT4B1-shR and SW620CSCs-OCT4B1-shR groups was lower than that in their control groups (Figures 4C and 4D). Furthermore, the same trend was observed for PLK1 protein levels detected by western blot (Figures 4E–4H). These results suggest that the *OCT4B1* gene in CSCs led to changes in the mRNA and protein expression levels of PLK1, which were consistent with the increase in mRNA and protein expression of OCT4B1 compared with those in the parental cancer cells. The silencing of the *OCT4B1* gene in shRNA-treated cells led to changes in PLK1 mRNA and protein expression levels, which were consistent with the decrease in OCT4B1 mRNA and protein expression.

Overexpressing PLK1 in SW480 Cells Induces EMT

Compared with that in the NC group, the protein expression of PLK1 in the SW480-PLK1 overexpression group significantly increased, and the difference was statistically significant (Figures 5A and 5B), suggesting that the *PLK1* gene was successfully overexpressed in the SW480-PLK1 group. Compared with the SW480-NC group, the expression of the epithelial cell marker E-cadherin in the SW480-PLK1 group significantly decreased, whereas the expression of the stromal cell markers N-cadherin and vimentin in the SW480-PLK1 group was significantly upregulated (Figures 5C and 5D). Accumulating research has documented that PLK1 can promote the expression of EMT transcription factors Twist1 and Slug and then induce the occurrence of EMT.[29] Therefore, we have detected Twist and Slug in this study. We found that the protein expression of Twist1 and Slug was increased in the SW480-PLK1 group compared with that in the SW480-NC group (Figures 5E and 5F), and these results suggested that PLK1 can induce the EMT process.

OCT4B1 Regulates miR-8064/PLK1 Balance

A differential gene expression cluster map of the SW480, SW480CSCs, SW480CSCs-NC, and SW480CSCs-OCT4B1-shR groups revealed the different miRNA expression patterns in the four groups of cells (Figure 6A). A total of 153 mRNAs were significantly downregulated in the SW480CSCs group, and a total of 266 mRNAs were significantly upregulated in the SW480CSCs-OCT4B1-shR group, with the criteria of 2-fold change and $p < 0.05$ (Tables S3 and S4). The scatter diagram illustrates cells in the four groups, with red and green showing differences of more than 3-fold in miRNA expression (Figure 6B). The results of a microarray (GSE119258) analysis revealed that the expression of the *OCT4B1* gene could cause abnormal expression of many miRNAs opposite to OCT4B1 and PLK1 in the four groups of cells (Figure S2), among which only miR-8064 was abnormally expressed and had binding sites in PLK1. miRNAs with PLK1 binding sites were predicted by TargetScan Human (http://www.targetscan.org/vert_71/). The results revealed 304 miRNA binding sites in PLK1, among which the binding sites of miR-8064 in PLK1 are shown in Figure 6C.

Furthermore, a dual-luciferase assay was used to determine whether PLK1 is the target gene of miR-8064. The pmiGLO/PLK1-3′ UTR and pmirGLO/PLK1-3′ UTR mut plasmids were constructed and

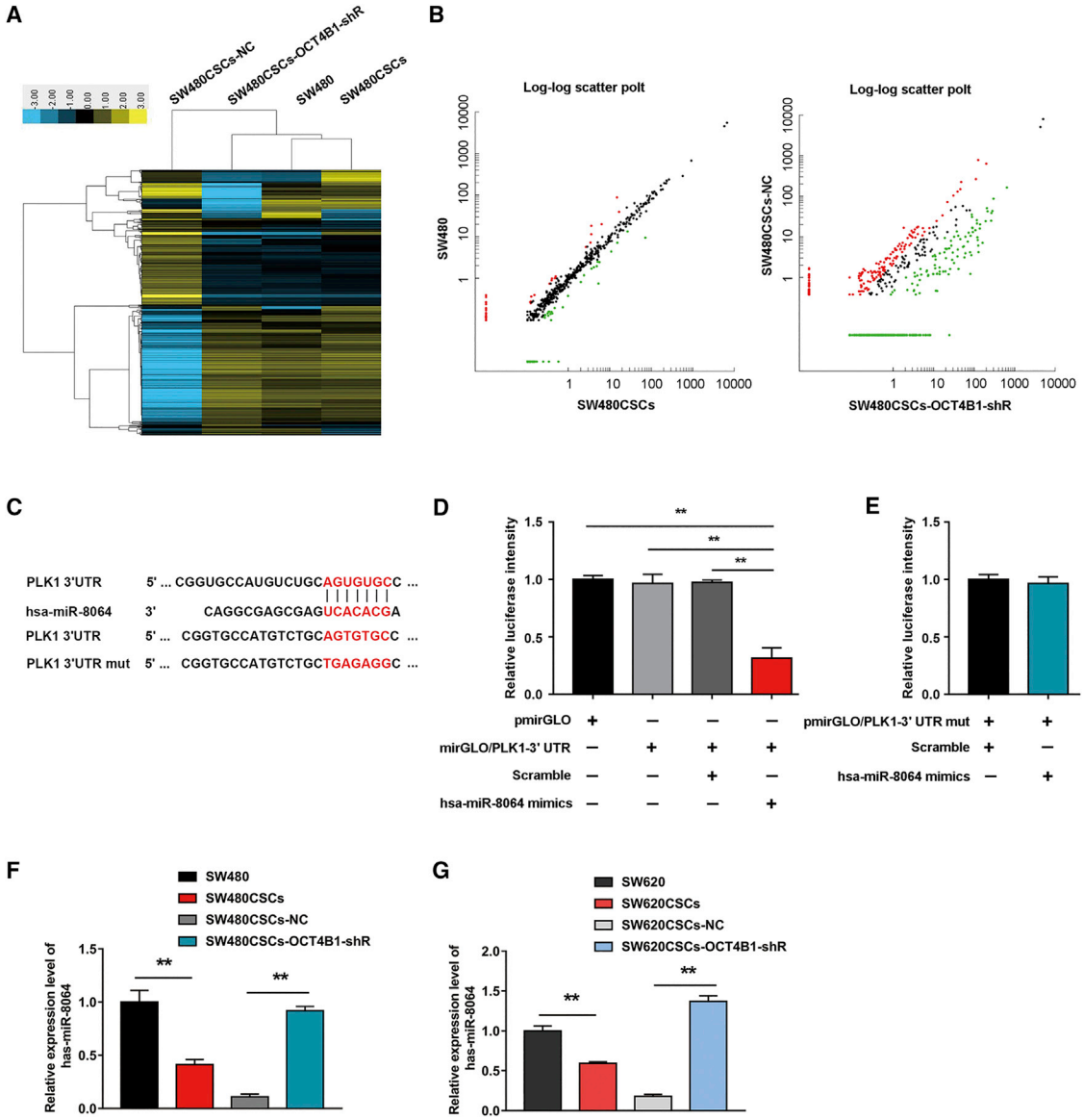

Figure 6. PLK1 Is the Direct Target Gene of miR-8064

(A) A cluster miRNA diagram showing all upregulated and downregulated miRNAs. (B) The difference in gene expression of each group is shown in the scatter diagram (labeled red for upregulated genes, labeled green for downregulated genes, and labeled black for no differences in gene expression). (C) The predicted binding sites of miR-8064 in the 3′ UTR of PLK1 were detected via a bioinformatics prediction tool (TargetScan Human). The mutated site in the 3′ UTR of PLK1 is shown. (D and E) A dual-fluorescence reporter assay verified that PLK1 is the direct target gene of miR-8064 (D, wild-type PLK1 3′ UTR fluorescent report experiment; E, mutated PLK1 3′ UTR fluorescent reporter experiment). (F) The relative expression of miR-8064 in the SW480, SW480CSCs, SW480CSCs-NC, and SW480CSCs-OCT4B1-shR groups was detected by qRT-PCR. (G) The relative expression of miR-8064 in the SW620, SW620CSCs, SW620CSCs-NC, and SW620CSCs-OCT4B1-shR groups was detected by qRT-PCR. Each bar represents the mean values ± SD of three independent experiments. **$p < 0.01$.

were transfected into the following six groups of cells: pmirGLO group, pmirGLO/PLK1-3′ UTR group, pmirGLO/PLK1-3′ UTR + miR-NC mimics group, pmirGLO/PLK1-3′ UTR + miR-8064 mimics group, pmirGLO/PLK1-3′ UTR mut + miR-NC mimics group, and pmirGLO/PLK1-3′ UTR mut + miR-8064 mimics group. The fluorescence changes in each group were detected using a fluorescence analyzer. The fluorescence intensity of the pmirGLO/PLK1-3′ UTR + miR-8064 mimics group was significantly lower than that of the other groups (Figures 6D and 6E). The dual-fluorescence reporter vector test revealed that PLK1 was the direct target gene of miR-8064.

Moreover, we verified the expression level of miR-8064 in cell lines with different levels of OCT4B1 gene expression. The relative expression of miR-8064 in the SW480, SW480CSCs, SW480CSCs-NC, and

SW480CSCs-OCT4B1-shR groups was 1.00 ± 0.12, 0.40 ± 0.06, 0.12 ± 0.03, and 0.93 ± 0.02, respectively, analyzed by qRT-PCR. The expression of miR-8064 in SW480CSCs was lower than that in the parental cancer cell line SW480, and the expression of miR-8064 in the SW480CSCs-OCT4B1-shR group was higher than that in the control group SW480CSCs-NC (Figure 6F). These results showed that the expression of miR-8064 in the four groups of cells was consistent with the results of the chip detection. In addition, the same trend was observed for the expression of miR-8064 in SW620, SW620CSCs, SW620CSCs-NC, and SW620CSCs-OCT4B1-shR groups as detected by qRT-PCR (Figure 6G). The above results suggest that OCT4B1 can negatively regulate miR-8064 expression in CRC cell lines. Because OCT4B1 positively regulates the expression of PLK1 and there is direct regulation between miR-8064 and PLK1, it could be concluded that OCT4B1 regulates miR-8064/PLK1 balance in CRC cell lines.

DISCUSSION

CSCs are considered subsets of cancer cells with high tumorigenicity, multilineage differentiation potential, self-renewal, and slow circulation.[6] Numerous studies have shown that spheres derived from cancer cell lines are enriched in CSCs as shown by culture of sphere stem cells.[30,31] The 3D microsphere model, which is formed by non-adherent growth through the addition of EGF, b-FGF, and B-27 in serum-free medium, theoretically contains a large amount of CSCs.[32,33] Colony formation experiments are the most reliable experiments for verifying cell growth and self-renewal.[34] CSCs can gain a clear clonal dominance *in vitro* and are more tumorigenic than parental cells. It was shown that CSCs were able to form tumors in NOD/SCID mice, whereas no significant tumor formation was observed in parental cells. The most common method to differentiate and identify CSCs is based on the unique glycoproteins on the cell surface. Accumulating evidence indicates that CD133 and CD44 are common markers of colorectal CSCs.[35,36] In our study, the percentages of CD133-positive cells and CD44-positive cells in 3D microspheres were significantly higher than those of the parental cells (Figures 1C and 1D). According to the high colony-forming ability, strong tumorigenicity, enrichment of tumor stem cell markers, and drug resistance, the suspension-cultured 3D microspheres were CSCs, which was consistent with Kaseb et al.'s[31] and Fan et al.'s[35] identification of CSCs.

OCT4B1 is mainly expressed in ESCs and embryonic carcinoma cells. Its main function is to maintain the pluripotency and self-renewal of stem cells.[23] In the present study, OCT4B1 expression was significantly increased in colorectal CSCs when compared with parental cells (Figure 1B). In combination with the significantly enhanced biological function of colorectal CSCs, EMT markers were detected, and it was found that the relative protein expression level of the epithelial cell marker E-cadherin was significantly reduced, and the relative protein expression levels of the mesenchymal cell markers N-cadherin and vimentin were significantly increased (Figures 2B and 2C). Hence the EMT process occurred. The objective was to investigate the role of OCT4B1 in the stem cell biological function of colorectal CSCs and its relationship with the EMT process. The *OCT4B1* gene was silenced in SW480CSCs and SW620CSCs by shRNA interference technology in order to successfully inhibit OCT4B1 in colorectal CSCs as determined by qRT-PCR and western blot analyses. This was able to indicate that OCT4B1 inhibition could reduce the colony formation ability of CRC, weaken tumor formation ability *in vivo*, and downregulate the expression of CSC markers. Furthermore, these results indicated that OCT4B1 played a key role in the stem cell biological properties of colorectal CSCs. Moreover, the relative protein expression of the epithelial cell marker E-cadherin significantly increased, and the relative protein expression of the mesenchymal cell markers N-cadherin and vimentin was significantly decreased (Figures 4A and 4B). This shows that the downregulation of the *OCT4B1* gene reduced the self-renewal of colorectal CSCs, and mesenchymal-epithelial transition (MET) occurred in reversing the EMT process. In our previous reports, cell migration and invasion were enhanced, and EMT marker changes were detected in SW480 and SW620 cells after overexpression of OCT4B1.[26]

Together with the previous study, the current study demonstrated that OCT4B1 can induce CRC cells to acquire self-renewal characteristics by promoting EMT processes. In addition, we analyzed OCT4B1 mRNA expression in surgical resection specimens derived from 53 CRC patients and found that OCT4B1 mRNA was correlated with the TNM stage ($p = 0.001$), tumor infiltration ($p = 0.013$), lymph node metastasis ($p = 0.014$), and distant metastasis ($p = 0.021$) of CRC (Table S2). Accumulating research has documented that EMT is associated with cancer progression and metastasis in CRC.[37,38] These results further supported the notion that OCT4B1 increased "EMT characteristics." Next, the underlying regulatory mechanisms will be discussed.

PLK1 is a serine or threonine protein kinase widely expressed in the human body that maintains chromosome stability, repairs damaged DNA, and prevents cell apoptosis by participating in cell mitosis in normal physiological processes.[39] PLK1 overexpression in numerous cancers is involved in the regulation of EMT.[29,40] Cai et al.[29] found that PLK1 promoted EMT and increased the metastasis of gastric cancer cells through the protein kinase B (AKT) signaling pathway. Wu et al.[40] found that PLK1 could promote cell migration and invasion by inducing EMT through the threonine kinase (CRAF)/signal-regulated kinase (ERK) signaling pathway in prostate cancer. Furthermore, some studies have suggested that PLK1 could also induce the EMT pathway indirectly through its substrate. In pancreatic cancer,[41] prostate cancer,[42] and gastric cancer,[43] PLK1 could further activate the FoxM1 direct target genes *Twist*, *Slug*, *Survivin*, and *Snail* through the direct binding and phosphorylation of FoxM1 and regulating the EMT process. Numerous studies have found that PLK1 overexpression in CRC cells leads to enhanced motility and invasiveness, and PLK1 overexpression in CRC tissues has been shown to be significantly associated with TNM stage, invasiveness, lymphatic metastasis, and worse survival, suggesting that abnormally elevated PLK1 may be a predictor of poor prognosis in CRC patients.[44–46]

We further detected the expression of PLK1 in cell lines with different levels of OCT4B1 expression. It was shown that the expression of OCT4B1 increased in colorectal CSCs, the self-renewal characteristics of colorectal CSCs significantly increased, and the EMT process occurred. Moreover, the mRNA and protein expression levels of PLK1 increased (Figures 4C–4H). By silencing the *OCT4B1* gene in colorectal CSCs, the expression of OCT4B1 was significantly decreased, the EMT process was reversed as the MET process, and the mRNA and protein expression of PLK1 decreased (Figures 4C–4H). Furthermore, the relative protein expression of the epithelial cell marker E-cadherin decreased, and the relative protein expression of the mesenchymal cell markers N-cadherin, vimentin, Twist, and Slug increased after overexpressing PLK1 in SW480 cells (Figures 5C–5F). These results suggest that PLK1 could induce the EMT process in SW480 cells, and these results are also consistent with previous reports.[29,40,41] It could be concluded that OCT4B1 could regulate PLK1 expression and promote EMT processes in CRC.

Accumulating research has found that a variety of miRNAs can regulate tumor cell proliferation, invasion, and apoptosis, as well as other related functions, by targeting PLK1 expression.[47–50] It has been demonstrated that miR-210 inhibits the proliferation of esophageal squamous cell carcinoma cells by inducing G2/M phase cell-cycle arrest, and this was mediated by targeting PLK1.[47] miR-296-5p inhibited cell viability by directly targeting PLK1 in non-small-cell lung cancers.[48] miR-100 could inhibit cell proliferation, induce apoptosis, arrest cell-cycle progression, and restore cisplatin sensitivity in epithelial ovarian cancers by targeting mechanistic target of rapamycin (mTOR) and PLK1 expression.[49] Recent research showed that the overexpression of miR-140 could inhibit the process of EMT and the invasion and migration of CRC.[50] It remains to be determined whether the miRNA targeting PLK1 in CRC plays a key role in the EMT process of CRC. By microarray screening, it was found that OCT4B1 could lead to an obvious change in the expression of miR-8064 (Figure S2), which was contrary to the expression pattern of OCT4B1 and PLK1, and that miR-8064 had a binding site in PLK1. Furthermore, dual-luciferase assay results verified that PLK1 was the downstream target gene of miR-8064 (Figures 6D and 6E). Moreover, compared with that in parental cells and OCT4B1-shR groups, the relative expression of miR-8064 in colorectal CSCs and CSCs-NC groups was significantly downregulated, as detected by qRT-PCR (Figures 6F and 6G), whereas the mRNA and protein expression of PLK1 detected by qRT-PCR and western blot, respectively, was significantly higher (Figures 4C–4H). These results demonstrated that OCT4B1 could regulate the balance of miR-8064/PLK1.

In conclusion, OCT4B1 may be involved in regulating the self-renewal of colorectal CSCs through EMT, which is at least partially due to the miR-8064/PLK1 balance. In addition, the present results provide a theoretical basis for targeted anticancer therapy, which is hoped to provide better treatment for patients with CRC and improve their prognosis and quality of life. However, the function of miR-8064 in CRC and its underlying mechanism require further investigation.

MATERIALS AND METHODS

Cell Culture and 3D Microsphere Culture

The human CRC cell lines SW480 and SW620 were purchased from the Cell Bank of the Chinese Academy of Sciences (Shanghai, China). 293T cells were purchased from Tianjin Saier Biotechnology (Tianjin, China). SW480, SW620, and 293T cell lines were grown in Leibovitz's L-15 medium (M&C GENE TECH, China) supplemented with 10% fetal bovine serum (FBS) (GIBCO, Australia), 100 U/mL penicillin, and 100 g/mL streptomycin (GIBCO, Australia). The cell lines were incubated at 37°C in a humidified atmosphere supplemented with 5% CO_2. The 3D microspheres were referred to as SW480-3D or SW620-3D microspheres. SW480 and SW620 cells with good cell growth and 80% confluency were washed three times with PBS and grown in serum-free Leibovitz's L-15 medium supplemented with key components of the stem cell culture medium: B27 (1:50; GIBCO, Australia), 20 ng/mL EGF (Invitrogen, USA), and 10 ng/mL bFGF (Invitrogen, USA). Three days after the replacement of the above medium to remove apoptotic cells, and after waiting until the medium color faded, an appropriate amount of stem cell culture medium was added in a timely manner. After the formation of good 3D microspheres, the specific gravity cell spheres were used, and the 3D microspheres and other floating dead cells were isolated and purified. The cell pellet continued to be cultured in the stem cell culture, which ultimately resulted in the 3D microspheres. When the volume of the microspheres increased approximately two times on average, relevant experiments were carried out.

Soft Agar Colony Formation Assay

Two concentrations of low-melting agarose solution (1.2% and 0.7%) were prepared with distilled water. After autoclaving, the solutions were stored in an oven at 42°C to prevent them from solidifying. The purified SW480-3D microspheres, SW620-3D microspheres, and parental cells SW480 and SW620, as well as the corresponding virus-interfering cells and NC group cells, were collected with Accutase enzyme (GIBCO, USA) and 0.25% trypsin (GIBCO, USA) for digestion of the single-cell suspension. Then, cells were counted, and the cell density was adjusted to 1×10^6 cells/L in L-15 culture medium containing 20% FBS. Then, 1.2% agarose and 20% FBS L-15 medium were mixed, 3 mL of the mixture was placed into a 6-cm-diameter glass dish, the mixture was cooled and allowed to solidify, and the CO_2 thermostat was placed on standby. Furthermore, 0.7% agarose and 20% FBS medium were mixed in a 1:1 ratio in a sterile tube, 0.5 mL of the cell suspension was added to the tube and thoroughly mixed, and poured into the 1.2% agarose plate to generate a solid double-agar layer. After 2 weeks of cell growth in soft agar, the number of colonies in each plate was counted using a light microscope, the number of colonies with >50 cells was recorded, and the clonogenic capacity was reflected by the rate of colony formation: Rate of colony formation = the number of cell clones/the number of seeded cells × 100%.

In Vivo Tumorigenicity

NOD/SCID mice and nude 6- to 8-week-old mice were purchased from the Experimental Animal Center of Chongqing Medical

University. Mice were acclimated for 1 week. Then, 1×10^3 of parental and 3D microsphere cells (SW480, SW480-3D microsphere, SW620, and SW620-microsphere cells) were suspended in 100 μL PBS and were subcutaneously injected into the left armpit of the NOD/SCID mice (five mice in each group). The mice were observed for up to 6 weeks and were sacrificed when the tumors reached a maximum diameter of 20 mm. A total of 1×10^6 SW480CSCs were treated with NC-GFP-LV or OCT4B1-shRNA-LV, mixed with 100 μL of PBS at 48 h postinfection, and injected into nude mice, as above. The tumor volumes were measured weekly, and the tumor size was calculated using the formula: volume = 1/2 (width^2 × length). After 6 weeks, the mice were sacrificed to check for tumor formation. All animal experiments were approved by the Ethics Committee for Animal Experimentation of Zunyi Medical University.

Flow Cytometry Analysis

For the flow cytometric analysis of CSC markers, cells were digested into single-cell suspensions and washed with PBS. Then, 1×10^6 cells were resuspended in 100 μL of PBS containing 0.5% BSA and 10 μL of fluorophore-conjugated primary antibody anti-CD133-phycoerythrin (PE) (Miltenyi Biotec, Germany) and anti-CD44-PE (Miltenyi Biotec, Germany) for 10 min in the dark at 4°C. Afterward, the tubes were removed by centrifugation and washed twice with 500 μL of PBS buffer. Next, cells were suspended in 200 μL of PBS and analyzed using a fluorescence-activated cell sorting (FACS) Vantage SE (BD Biosciences, Franklin Lakes, USA).

qRT-PCR

Total RNA was isolated with a total RNA extraction kit (Solarbio, Beijing, China) according to the manufacturer's instructions. RNA concentrations were determined using a NanoDrop instrument (NanoDrop Technologies, Wilmington, DE, USA). RNA was reverse transcribed to cDNA with the PrimeScript RT Reagent Kit (TAKARA, Dalian, China) according to the manufacturer's instructions. Real-time PCR was carried out with the CFX96 Real-Time System (Bio-Rad, USA) with a 25 μL reaction mixture containing 12.5 μL of qPCR SYBR Green Mix (TAKARA, Dalian, China), 0.4 μM of each primer, 1 μL of cDNA, and diethyl pyrocarbonate-treated H_2O up to the final volume. The forward and reverse primers were synthesized by Dalian Bao Biotech (Table S1). Gene expression levels were quantified using the Bio-Rad CFX96 detection system, and the samples were normalized by GAPDH or U6 expression levels. Relative expression was calculated using the $2-\Delta\Delta$Ct method.

Western Blot Assay

Western blotting was performed on cytosolic cellular extracts. Equal amounts of protein were resolved under reducing conditions in 10% SDS-PAGE gels. Protein migration was assessed using protein standards (Bio-Rad, USA). The transfer onto a nitrocellulose blot was performed overnight at 30 V using a wet transfer system. Equal protein loading was confirmed through Ponceau staining. The blot was blocked in 5% skim milk in TBS plus 0.03% Tween 20 (TBST) for 1 h and incubated overnight at 4°C with anti-E-cadherin (1:1,000; Abcam, Cambridge, UK), anti-N-cadherin (1:1,000; Abcam, Cambridge, UK), anti-vimentin (1:1,000; Abcam, Cambridge, UK), anti-P-gp (1:1,000; Cell Signaling Technology), anti-ABCG2 (1:1,000; Cell Signaling Technology), anti-Twist (1:1,000; Cell Signaling Technology), anti-Slug (1:1,000; Cell Signaling Technology), anti-CD44 (1:1,000; Abcam, Cambridge, UK), anti-CD133 (1:1,000; Abcam, Cambridge, UK), anti-PLK1 (1:1,000; Abcam, Cambridge, UK), anti-β-tubulin (1:1,000; Abcam, Cambridge, UK), and anti-GAPDH (1:2,000; Abcam, Cambridge, UK). Then, the blot was washed with TBST and subsequently incubated in a horseradish peroxidase-conjugated antibody solution (1:5,000; Amersham Life Sciences, Piscataway, NJ, USA) for 1 h at room temperature. Protein bands were visualized using a chemiluminescent substrate and exposing the blot to autoradiographic film. LabWorks Image Acquisition and Analysis software (UvP) was used to quantify the band intensities.

Cell Transfection

Lentiviral constructs expressing OCT4B1 shRNA (OCT4B1-shRNA-LV) were purchased from Shanghai Genechem, China. The OCT4B1 shRNA vector sequence was as follows: 5′-GATCCCAGACT ACCCTCACCCATGTTCAAGAGACATGGGTGAGGGTAGTCTG TTTTTTGGAAA-3′; reverse: 5′-AGCTTTTCCAAAAAACAGAC TACCCTCACCCATGTCTCTTGAACATGGGTGAGGGTAGTCT GCG-3′. SW480 and SW620 cells were seeded in a six-well plate at a concentration of 2×10^5 cells per well (30% confluence) on the day before shRNA transduction. OCT4B1-shRNA-LV was transduced into cells at a MOI of 20 (SW480) or 30 (SW620) using Polybrene (8 mg/mL) and Enhanced Infection Solution (Genechem, China). At the same time, a nontarget NC virus GFP-LV (Genechem, China) was transduced into cells using the same methods to control for the effects of the viral vector. To exclude effects of the virus plasmid vector, we included an NC group transfected with an NC virus (NC-GFP-LV; purchased from Genechem, Shanghai, China) in the experiment. After incubation for 12 h, the medium was replaced with fresh L-15 medium. The transduction efficiencies were observed using a fluorescence microscopy camera at 72 h after transduction. The generation of overexpression lentivirus (PLK1-GFP-PURO virus) and NC virus (GFP-PURO virus) was performed by Shanghai Genechem, China. The optimal transfection conditions were obtained in a pre-experiment (MOI = 40, 2 mg/mL Polybrene), and SW480 cells were transfected at the optimal number and growth state. At the indicated time points, cells were harvested for mRNA and protein analysis, as well as for other assays.

Patients and Tissue Samples

Fifty-three primary CRC tissue specimens were consecutively collected from patients undergoing curative resection in 2019 between January and March at the Affiliated Hospital of Zunyi Medical University (Zunyi, China). Specimens were frozen in liquid nitrogen immediately after surgical removal and were stored in liquid nitrogen until use for qRT-PCR analysis. The clinicopathological characteristics of the 53 primary CRC cases were as follows: mean age was 58.3 (range 34–81) years; 30 males and 23 females; and 14 were well differentiated, 31 moderately differentiated, and 8 poorly

differentiated. Pathological TNM staging was performed according to the 8th edition of the Union for International Cancer Control (UICC) as follows: 5 stage I, 16 stage II, 27 stage III, and 5 stage IV. The diagnosis of CRC was established based on histopathological evaluation. Written informed consent was obtained from all patients. The study was approved by the Ethics Committee of the Affiliated Hospital of Zunyi Medical University. Signed informed consent was obtained from the patients or their guardians.

Microarray Analysis

Total RNA was isolated from SW480, SW480CSCs, SW480CSCs-NC, and SW480CSCs-OCT4B1-shR group cells using a total RNA extraction kit (Solarbio, Beijing, China) according to the manufacturer's instructions. Total RNA was purified using the mirVana miRNA Isolation Kit (AM1561). Purified RNA was dephosphorylated and labeled using the miRNA Complete Labeling and Hyb Kit (Agilent, USA). The chips were scanned using the Agilent chip scanner (G2565CA) to obtain hybrid images. Agilent Feature Extraction software (v10.7) was used to analyze acquired hybrid images; differentially expressed genes with statistical significance among the four groups were identified through Volcano Plot filtering. Differentially expressed genes among the four samples were identified through fold change filtering. Hierarchical clustering was performed using R scripts. GO analysis was performed using the standard enrichment computation method. Global Gene expression array data are available at the NCBI GEO under accession number GEO: GSE119258 (https://www.ncbi.nlm.nih.gov/geo/query/acc.cgi?acc=GSE119258).

Dual-Luciferase Reporter Assay

After construction of pmirGLO/PLK1-3′ UTR and pmirGLO/PLK1-3′ UTR mut vectors, cells were divided into six groups, according to the different transfection conditions: pmirGLO group, pmirGLO/PLK1-3′ UTR group, pmirGLO/PLK1-3′ UTR + miR-NC mimics group, pmirGLO/PLK1-3′ UTR + miR-8064 mimics group, pmirGLO/PLK1- 3′ UTR mut + miR-NC mimics group, and pmirGLO/PLK1-3′ UTR mut + miR-8064 mimics group. For cell transfection, 293T cells were digested and centrifuged before transfection and inoculated into a 48-well plate with 6×10^4 cells per well. The first transfection was performed in the miRNA-NC mimic group as an example as follows: transfection solutions A and B were prepared, with transfection solution A containing 1 μL (20 μM) of the miRNA-NC mimic diluted with 49 μL of serum-free medium and mixed well, and transfection solution B containing 1 μL (20 μM) of Lipofectamine 2000 reagent diluted with 49 μL of L-15 serum-free medium and mixed well at room temperature for 5 min. Transfection solution B was mixed with transfection solution A and was placed at room temperature for 20 min. Then, the configured transfection medium was added to the corresponding plates (100 μL/well), cultured in an incubator for 4 h, and added to the common medium (3 mL/well), and the cells were cultured further. The second transfection was performed as follows. A 1.5-mL centrifuge tube was used to prepare transfection solutions A and B. L-15 serum-free medium was added and diluted with 0.4 g of pmirGLO or pmirGLO/PLK1-3′ UTR at a total of 50 L of mixed liquid. To make solution B, L-15 serum-free medium was added and diluted with 0.4 μL of Lipofectamine 2000 Reagent to a final volume of 50 μL after mixing at room temperature for 5 min. Solution B was mixed with solution A after incubation at room temperature for 20 min. The transfection liquid was added to the corresponding wells (100 μL/well) after incubation for 4 h and was added to the common medium (3 mL/well), and the cells were cultured further. The Dual-Luciferase Reporter Gene Test Kit (Beyotime Biotechnology, Shanghai, China) was used to detect luciferase activities in different groups after 48 h of cotransfection. The firefly and Renilla luciferase reagents were added to detect the luciferase activity of each group.

Statistical Analysis

Data were expressed as the mean ± SD. Comparisons between the two groups were analyzed by Student's t test. For testing among multiple groups, one-way ANOVA with the Student-Newman-Keuls (SNK)-q test was conducted. The Pearson χ^2 test was performed to analyze the relationship between OCT4B1 mRNA expression and the clinicopathological characteristics. Statistical analyses were performed using SPSS software (version 18.0). Each experiment was performed three times, and $p < 0.05$ was considered statistically significant.

SUPPLEMENTAL INFORMATION

Supplemental Information can be found online at https://doi.org/10.1016/j.omto.2019.08.004.

AUTHOR CONTRIBUTIONS

J.-m.Z., S.-q.H., and K.-m.W. conceived and designed the experiments. J.-m.Z., S.-q.H., H.J., Y.-l.C., and Z.-q.C. performed the experiments and statistical data analysis. J.-m.Z., S.-q.H., J.-h.F., and K.-m.W. participated in the discussion and interpretation of data. J.-m.Z. wrote the paper. K.-m.W. supervised all experimental work. All authors read and approved the final manuscript.

CONFLICTS OF INTEREST

The authors declare no competing interests.

ACKNOWLEDGMENTS

We thank the Department of Immunology, Zunyi Medical University for providing the experimental platform. This work was supported by the National Natural Science Foundation of China (grants 81260369 and 81560404) and the Science and Technology Fund Foundation of Guizhou (grant [2015]7453).

REFERENCES

1. Bray, F., Ferlay, J., Soerjomataram, I., Siegel, R.L., Torre, L.A., and Jemal, A. (2018). Global cancer statistics 2018: GLOBOCAN estimates of incidence and mortality worldwide for 36 cancers in 185 countries. CA Cancer J. Clin. *68*, 394–424.

2. Siegel, R.L., Miller, K.D., Fedewa, S.A., Ahnen, D.J., Meester, R.G.S., Barzi, A., and Jemal, A. (2017). Colorectal cancer statistics, 2017. CA Cancer J. Clin. *67*, 177–193.

3. Miller, K.D., Siegel, R.L., Lin, C.C., Mariotto, A.B., Kramer, J.L., Rowland, J.H., Stein, K.D., Alteri, R., and Jemal, A. (2016). Cancer treatment and survivorship statistics, 2016. CA Cancer J. Clin. *66*, 271–289.

4. Bao, B., Ahmad, A., Azmi, A.S., Ali, S., and Sarkar, F.H. (2013). Overview of cancer stem cells (CSCs) and mechanisms of their regulation: implications for cancer therapy. Curr. Protoc. Pharmacol. *61*, 14.25.1–14.25.14.

5. Mitra, A., Mishra, L., and Li, S. (2015). EMT, CTCs and CSCs in tumor relapse and drug-resistance. Oncotarget *6*, 10697–10711.

6. Lobo, N.A., Shimono, Y., Qian, D., and Clarke, M.F. (2007). The biology of cancer stem cells. Annu. Rev. Cell Dev. Biol. *23*, 675–699.

7. Ajani, J.A., Song, S., Hochster, H.S., and Steinberg, I.B. (2015). Cancer stem cells: the promise and the potential. Semin. Oncol. *42* (*Suppl 1*), S3–S17.

8. Shibue, T., and Weinberg, R.A. (2017). EMT, CSCs, and drug resistance: the mechanistic link and clinical implications. Nat. Rev. Clin. Oncol. *14*, 611–629.

9. Nieto, M.A., Huang, R.Y., Jackson, R.A., and Thiery, J.P. (2016). EMT: 2016. Cell *166*, 21–45.

10. Charpentier, M., and Martin, S. (2013). Interplay of Stem Cell Characteristics, EMT, and Microtentacles in Circulating Breast Tumor Cells. Cancers (Basel) *5*, 1545–1565.

11. Scheel, C., Eaton, E.N., Li, S.H., Chaffer, C.L., Reinhardt, F., Kah, K.J., Bell, G., Guo, W., Rubin, J., Richardson, A.L., and Weinberg, R.A. (2011). Paracrine and autocrine signals induce and maintain mesenchymal and stem cell states in the breast. Cell *145*, 926–940.

12. Lee, J.H., Kim, J.Y., Kim, S.Y., Choi, S.I., Kim, K.C., Cho, E.W., and Kim, I.G. (2017). APBB1 reinforces cancer stem cell and epithelial-to-mesenchymal transition by regulating the IGF1R signaling pathway in non-small-cell lung cancer cells. Biochem. Biophys. Res. Commun. *482*, 35–42.

13. Liu, F., Kong, X., Lv, L., and Gao, J. (2015). TGF-β1 acts through miR-155 to down-regulate TP53INP1 in promoting epithelial-mesenchymal transition and cancer stem cell phenotypes. Cancer Lett. *359*, 288–298.

14. Grosse-Wilde, A., Fouquier d'Hérouël, A., McIntosh, E., Ertaylan, G., Skupin, A., Kuestner, R.E., del Sol, A., Walters, K.A., and Huang, S. (2015). Stemness of the hybrid Epithelial/Mesenchymal State in Breast Cancer and Its Association with Poor Survival. PLoS ONE *10*, e0126522.

15. Cavnar, M.J., Zeng, S., Kim, T.S., Sorenson, E.C., Ocuin, L.M., Balachandran, V.P., Seifert, A.M., Greer, J.B., Popow, R., Crawley, M.H., et al. (2013). KIT oncogene inhibition drives intratumoral macrophage M2 polarization. J. Exp. Med. *210*, 2873–2886.

16. Smith, B.N., and Bhowmick, N.A. (2016). Role of EMT in Metastasis and Therapy Resistance. J. Clin. Med. *5*, e17.

17. Wen, K., Fu, Z., Wu, X., Feng, J., Chen, W., and Qian, J. (2013). Oct-4 is required for an antiapoptotic behavior of chemoresistant colorectal cancer cells enriched for cancer stem cells: effects associated with STAT3/Survivin. Cancer Lett. *333*, 56–65.

18. Almozyan, S., Colak, D., Mansour, F., Alaiya, A., Al-Harazi, O., Qattan, A., Al-Mohanna, F., Al-Alwan, M., and Ghebeh, H. (2017). PD-L1 promotes OCT4 and Nanog expression in breast cancer stem cells by sustaining PI3K/AKT pathway activation. Int. J. Cancer *141*, 1402–1412.

19. Sun, L., Liu, T., Zhang, S., Guo, K., and Liu, Y. (2017). Oct4 induces EMT through LEF1/β-catenin dependent WNT signaling pathway in hepatocellular carcinoma. Oncol. Lett. *13*, 2599–2606.

20. Gazouli, M., Roubelakis, M.G., Theodoropoulos, G.E., Papailiou, J., Vaiopoulou, A., Pappa, K.I., Nikiteas, N., and Anagnou, N.P. (2012). OCT4 spliced variant OCT4B1 is expressed in human colorectal cancer. Mol. Carcinog. *51*, 165–173.

21. Atlasi, Y., Mowla, S.J., Ziaee, S.A., Gokhale, P.J., and Andrews, P.W. (2008). OCT4 spliced variants are differentially expressed in human pluripotent and nonpluripotent cells. Stem Cells *26*, 3068–3074.

22. Asadi, M.H., Mowla, S.J., Fathi, F., Aleyasin, A., Asadzadeh, J., and Atlasi, Y. (2011). OCT4B1, a novel spliced variant of OCT4, is highly expressed in gastric cancer and acts as an antiapoptotic factor. Int. J. Cancer *128*, 2645–2652.

23. Farashahi Yazd, E., Rafiee, M.R., Soleimani, M., Tavallaei, M., Salmani, M.K., and Mowla, S.J. (2011). OCT4B1, a novel spliced variant of OCT4, generates a stable truncated protein with a potential role in stress response. Cancer Lett. *309*, 170–175.

24. Papamichos, S.I., Kotoula, V., Tarlatzis, B.C., Agorastos, T., Papazisis, K., and Lambropoulos, A.F. (2009). OCT4B1 isoform: the novel OCT4 alternative spliced variant as a putative marker of stemness. Mol. Hum. Reprod. *15*, 269–270.

25. Mirzaei, M.R., Najafi, A., Arababadi, M.K., Asadi, M.H., and Mowla, S.J. (2014). Altered expression of apoptotic genes in response to OCT4B1 suppression in human tumor cell lines. Tumour Biol. *35*, 9999–10009.

26. Wen, K.M., Zhang, G.H., Li, J., Chen, Z.Q., Cheng, Y.L., Su, X., and Zeng, Q.L. (2015). OCT4B1 promotes cell growth, migration and invasion suppressing sensitivity to oxaliplatin in colon cancer. Oncol. Rep. *34*, 2943–2952.

27. Chen, B., Zhang, D., Kuai, J., Cheng, M., Fang, X., and Li, G. (2017). Upregulation of miR-199a/b contributes to cisplatin resistance via Wnt/β-catenin-ABCG2 signaling pathway in ALDHA1^{+} colorectal cancer stem cells. Tumour Biol. *39*, 1010428317715155.

28. Jin, Y., Wang, M., Hu, H., Huang, Q., Chen, Y., and Wang, G. (2018). Overcoming stemness and chemoresistance in colorectal cancer through miR-195-5p-modulated inhibition of notch signaling. Int. J. Biol. Macromol. *117*, 445–453.

29. Cai, X.P., Chen, L.D., Song, H.B., Zhang, C.X., Yuan, Z.W., and Xiang, Z.X. (2016). PLK1 promotes epithelial-mesenchymal transition and metastasis of gastric carcinoma cells. Am. J. Transl. Res. *8*, 4172–4183.

30. Zhong, Y., Guan, K., Guo, S., Zhou, C., Wang, D., Ma, W., Zhang, Y., Li, C., and Zhang, S. (2010). Spheres derived from the human SK-RC-42 renal cell carcinoma cell line are enriched in cancer stem cells. Cancer Lett. *299*, 150–160.

31. Kaseb, H.O., Fohrer-Ting, H., Lewis, D.W., Lagasse, E., and Gollin, S.M. (2016). Identification, expansion and characterization of cancer cells with stem cell properties from head and neck squamous cell carcinomas. Exp. Cell Res. *348*, 75–86.

32. Bussolati, B., Bruno, S., Grange, C., Buttiglieri, S., Deregibus, M.C., Cantino, D., and Camussi, G. (2005). Isolation of renal progenitor cells from adult human kidney. Am. J. Pathol. *166*, 545–555.

33. Pisanu, M.E., Noto, A., De Vitis, C., Masiello, M.G., Coluccia, P., Proietti, S., Giovagnoli, M.R., Ricci, A., Giarnieri, E., Cucina, A., et al. (2014). Lung cancer stem cell lose their stemness default state after exposure to microgravity. BioMed Res. Int. *2014*, 470253.

34. Borowicz, S., Van Scoyk, M., Avasarala, S., Karuppusamy Rathinam, M.K., Tauler, J., Bikkavilli, R.K., and Winn, R.A. (2014). The soft agar colony formation assay. J. Vis. Exp. *92*, e51998.

35. Fan, F., Bellister, S., Lu, J., Ye, X., Boulbes, D.R., Tozzi, F., Sceusi, E., Kopetz, S., Tian, F., Xia, L., et al. (2015). The requirement for freshly isolated human colorectal cancer (CRC) cells in isolating CRC stem cells. Br. J. Cancer *112*, 539–546.

36. Dalerba, P., Dylla, S.J., Park, I.K., Liu, R., Wang, X., Cho, R.W., Hoey, T., Gurney, A., Huang, E.H., Simeone, D.M., et al. (2007). Phenotypic characterization of human colorectal cancer stem cells. Proc. Natl. Acad. Sci. USA *104*, 10158–10163.

37. Vu, T., and Datta, P.K. (2017). Regulation of EMT in Colorectal Cancer: A Culprit in Metastasis. Cancers (Basel) *9*, e171.

38. Sun, J., Zhang, T., Cheng, M., Hong, L., Zhang, C., Xie, M., Sun, P., Fan, R., Wang, Z., Wang, L., and Zhong, J. (2019). TRIM29 facilitates the epithelial-to-mesenchymal transition and the progression of colorectal cancer via the activation of the Wnt/β-catenin signaling pathway. J. Exp. Clin. Cancer Res. *38*, 104.

39. Helmke, C., Becker, S., and Strebhardt, K. (2016). The role of Plk3 in oncogenesis. Oncogene *35*, 135–147.

40. Wu, J., Ivanov, A.I., Fisher, P.B., and Fu, Z. (2016). Polo-like kinase 1 induces epithelial-to-mesenchymal transition and promotes epithelial cell motility by activating CRAF/ERK signaling. eLife *5*, e10734.

41. Huang, C., Xie, D., Cui, J., Li, Q., Gao, Y., and Xie, K. (2014). FOXM1c promotes pancreatic cancer epithelial-to-mesenchymal transition and metastasis via upregulation of expression of the urokinase plasminogen activator system. Clin. Cancer Res. *20*, 1477–1488.

42. Wang, Y., Yao, B., Wang, Y., Zhang, M., Fu, S., Gao, H., Peng, R., Zhang, L., and Tang, J. (2014). Increased FoxM1 expression is a target for metformin in the suppression of EMT in prostate cancer. Int. J. Mol. Med. *33*, 1514–1522.

43. Miao, L., Xiong, X., Lin, Y., Cheng, Y., Lu, J., Zhang, J., and Cheng, N. (2014). Down-regulation of FoxM1 leads to the inhibition of the epithelial-mesenchymal transition in gastric cancer cells. Cancer Genet. *207*, 75–82.

44. Takahashi, T., Sano, B., Nagata, T., Kato, H., Sugiyama, Y., Kunieda, K., Kimura, M., Okano, Y., and Saji, S. (2003). Polo-like kinase 1 (PLK1) is overexpressed in primary colorectal cancers. Cancer Sci. *94*, 148–152.

45. Tut, T.G., Lim, S.H., Dissanayake, I.U., Descallar, J., Chua, W., Ng, W., de Souza, P., Shin, J.S., and Lee, C.S. (2015). Upregulated Polo-Like Kinase 1 Expression Correlates with Inferior Survival Outcomes in Rectal Cancer. PLoS ONE *10*, e0129313.

46. Han, D.P., Zhu, Q.L., Cui, J.T., Wang, P.X., Qu, S., Cao, Q.F., Zong, Y.P., Feng, B., Zheng, M.H., and Lu, A.G. (2012). Polo-like kinase 1 is overexpressed in colorectal cancer and participates in the migration and invasion of colorectal cancer cells. Med. Sci. Monit. *18*, BR237–BR246.

47. Li, C., Zhou, X., Wang, Y., Jing, S., Yang, C., Sun, G., Liu, Q., Cheng, Y., and Wang, L. (2014). miR-210 regulates esophageal cancer cell proliferation by inducing G2/M phase cell cycle arrest through targeting PLK1. Mol. Med. Rep. *10*, 2099–2104.

48. Xu, C., Li, S., Chen, T., Hu, H., Ding, C., Xu, Z., Chen, J., Liu, Z., Lei, Z., Zhang, H.T., et al. (2016). miR-296-5p suppresses cell viability by directly targeting PLK1 in non-small cell lung cancer. Oncol. Rep. *35*, 497–503.

49. Guo, P., Xiong, X., Zhang, S., and Peng, D. (2016). miR-100 resensitizes resistant epithelial ovarian cancer to cisplatin. Oncol. Rep. *36*, 3552–3558.

50. Li, J., Zou, K., Yu, L., Zhao, W., Lu, Y., Mao, J., Wang, B., Wang, L., Fan, S., Song, B., and Li, L. (2018). MicroRNA-140 Inhibits the Epithelial-Mesenchymal Transition and Metastasis in Colorectal Cancer. Mol. Ther. Nucleic Acids *10*, 426–437.